European and Mediterranean hydroclimate responses to tropical volcanic forcing over the last millennium

M. P. Rao[1,2] (iD), B. I. Cook[3,4] (iD), E. R. Cook[1], R. D. D'Arrigo[1], P. J. Krusic[5,6] (iD), K. J. Anchukaitis[7] (iD), A. N. LeGrande[3] (iD), B. M. Buckley[1] (iD), N. K. Davi[1,8], C. Leland[1,2] (iD), and K. L. Griffin[2,9] (iD)

[1]Tree Ring Laboratory, Lamont-Doherty Earth Observatory of Columbia University, Palisades, New York, USA, [2]Department of Earth and Environmental Sciences, Columbia University, New York, New York, USA, [3]NASA Goddard Institute for Space Studies, New York, New York, USA, [4]Ocean and Climate Physics, Lamont-Doherty Earth Observatory of Columbia University, Palisades, New York, USA, [5]Department of Geography, University of Cambridge, Cambridge, UK, [6]Department of Physical Geography, Stockholm University, Stockholm, Sweden, [7]Laboratory of Tree Ring Research, University of Arizona, Tucson, Arizona, USA, [8]Department of Environmental Science, William Paterson University, Wayne, New Jersey, USA, [9]Ecology, Evolution and Environmental Biology, Columbia University, New York, New York, USA

Abstract Volcanic eruptions have global climate impacts, but their effect on the hydrologic cycle is poorly understood. We use a modified version of superposed epoch analysis, an eruption year list collated from multiple data sets, and seasonal paleoclimate reconstructions (soil moisture, precipitation, geopotential heights, and temperature) to investigate volcanic forcing of spring and summer hydroclimate over Europe and the Mediterranean over the last millennium. In the western Mediterranean, wet conditions occur in the eruption year and the following 3 years. Conversely, northwestern Europe and the British Isles experience dry conditions in response to volcanic eruptions, with the largest moisture deficits in posteruption years 2 and 3. The precipitation response occurs primarily in late spring and early summer (April–July), a pattern that strongly resembles the negative phase of the East Atlantic Pattern. Modulated by this mode of climate variability, eruptions force significant, widespread, and heterogeneous hydroclimate responses across Europe and the Mediterranean.

1. Introduction

Large volcanic eruptions can inject sulfur dioxide into the stratosphere where it is converted into aerosolized sulfuric acid. These aerosols can persist in the stratosphere for several years, where they reflect and absorb incoming solar radiation, cooling global surface temperatures but warming the stratosphere [*Robock*, 2000]. Volcanic eruptions are therefore useful events to study the response of Earth's climate system to short-term changes in radiative forcing. However, the temperature effects of volcanic forcing have received considerable attention [e.g., *Anchukaitis et al.*, 2012, 2017; *D'Arrigo et al.*, 2009; *Luterbacher and Pfister*, 2015; *Meehl et al.*, 2004; *Stoffel et al.*, 2015] and are relatively better constrained than the hydroclimate response [*Anchukaitis et al.*, 2010; *Broccoli et al.*, 2003; *Iles and Hegerl*, 2014].

Modeling and observational studies find a global decrease in precipitation in the immediate years following volcanic events [e.g., *Iles et al.*, 2013; *Joseph and Zeng*, 2011], although the regional- and seasonal-scale responses are more nuanced [*Anchukaitis et al.*, 2010; *Fischer et al.*, 2007b]. The decrease in global precipitation is likely caused by the reduction of incident shortwave radiation at the surface due to stratospheric volcanic aerosols, suppressing evaporation and leading to a cooler and more stable troposphere [*Iles and Hegerl*, 2014]. However, many of these studies focus on the past century when instrumental climate data are available or are based on climate model outputs. In terms of global radiative forcing, there have only been two major volcanic eruptions during the past half century, El Chichón in 1982, and Mount Pinatubo in 1991, both of which coincided with El Niño events. Consequently, our understanding of the climate system's response to multiple eruptions over the past millennium is extremely limited.

Over Europe, the winter hydroclimate response to volcanic forcing resembles a positive phase of the North Atlantic Oscillation (NAO) [e.g., *Driscoll et al.*, 2012; *Shindell et al.*, 2004; *Zanchettin et al.*, 2013]. Less is known, however, about the effect of volcanic eruptions on spring and summer hydroclimate. The response may be further complicated by the influence of various modes of climate variability on interannual and decadal

timescales over Europe and the Mediterranean. These include the winter and spring NAO, the East Atlantic Pattern (EAP), the East-Atlantic-Scandinavian Pattern, the East-Atlantic West-Russia Pattern (EAWR) [*Barnston and Livezey*, 1987; *Schrier et al.*, 2006], and the summertime parallel of the winter NAO known as the summer NAO (SNAO) [*Folland et al.*, 2009].

Here we investigate the spatiotemporal hydroclimate response to volcanic eruptions over Europe and the Mediterranean using a modified version of superposed epoch analysis (SEA) and test whether volcanism modulates spring and summer hydroclimate through variability in the aforementioned climatic modes. Our modified SEA generates multiple unique draws of key years and determines the volcanic response in a probabilistic framework, allowing us to present uncertainty estimates in this response. We expand on previous analyses [*Fischer et al.*, 2007b] using updated volcanic forcing data and investigate the hydroclimate response in a new, longer (1100–2012 Common Era (C.E.)) hydroclimate reconstruction: the tree ring-based "Old World Drought Atlas" or OWDA [*Cook et al.*, 2015] that allows assessment of the response over a greatly expanded list of event years. Further, we extensively evaluate the seasonality of climatic anomalies and teleconnections forcings that may modulate this observed response [cf. *Büntgen et al.*, 2017; *Gao and Gao*, 2017]. We compare the OWDA response to a largely independent multiproxy seasonal precipitation reconstruction (1500–2000 C.E.) [*Pauling et al.*, 2006] and a recent temperature reconstruction (755–2003 C.E.) [*Luterbacher et al.*, 2016].

2. Data and Methods

2.1. Data

Estimates of past hydroclimate variability over Europe and the Mediterranean are from the OWDA [*Cook et al.*, 2015], a gridded tree ring-based reconstruction of mean June through August (JJA) self-calibrating Palmer Drought Severity Index (PDSI) [*Palmer*, 1965; *Schrier et al.*, 2013]. Along with the OWDA we use a gridded multiproxy seasonal precipitation reconstruction for Europe [*Pauling et al.*, 2006] and a summer (JJA) European temperature reconstruction [*Luterbacher et al.*, 2016]. See Text S1 in the supporting information [*Cook et al.*, 1999; *Dai*, 2011; *Fritts*, 1976; *George et al.*, 2010] for more details on the OWDA and *Pauling et al.* [2006] reconstructions. Other data sets used include National Center for Atmospheric Research-National Center for Environmental Prediction (NCAR-NCEP) mean monthly sea level pressure (MSLP) [*Kalnay et al.*, 1996], gridded Climate Research Unit (CRU) TS 3.21 precipitation and temperature [*Harris et al.*, 2014], and National Oceanic and Atmospheric Administration-Climate Prediction Centre (NOAA-CPC) NAO, EAP, and EAWR indices. To develop a "key year list" of volcanic eruptions, we compile data from five volcanic event lists (Table S1), generated by analyzing sulfate loading in bipolar ice cores [*Crowley and Unterman*, 2013; *Gao et al.*, 2008; *Plummer et al.*, 2012; *Sigl et al.*, 2013, 2015].

2.2. Analysis

To facilitate the interpretation of volcanically forced hydroclimate anomalies, we first examine the seasonality of climate signals integrated by the OWDA, along with the relationship between regional precipitation and temperature. We do this by calculating the spatial field correlation between the OWDA and gridded climate data (CRU precipitation and temperature) and the spatial field correlation between the two gridded climate data sets themselves (see Text S1). Next, we use SEA to determine the statistical significance of volcanically forced climatic anomalies [e.g., *Adams et al.*, 2003; *Anchukaitis et al.*, 2010; *Fischer et al.*, 2007b]. The SEA is a statistical method to identify consistent responses to events, by testing for the possibility of random occurrence [*Haurwitz and Brier*, 1981]. One assumption of the SEA however is that the key year list (volcanic event years in our case) is accurate [*Zanchettin et al.*, 2013], when, in fact, there are uncertainties associated with estimates of volcanic event years from ice core evidence [*Baillie*, 2008; *Plummer et al.*, 2012; *Sigl et al.*, 2015]. Additionally, conventional SEA does not provide response uncertainty estimates based on the choice of key years.

We estimate the volcanic response using ($n_1 = 1000$) unique subsets of eruption years from the key year list in Table S1. Each subset is the mean response of $n_2 = 10$ key years. Next, we determine the median, 10th and 90th percentiles of these ($n_1 = 1000$) mean responses on a grid cell basis, providing an estimate of the sensitivity of the observed response to the choice of key event years, and the widest possible uncertainty estimate based on this choice. For each of the 10 years in the 1000 draws of nonrepeating subsets, we study the
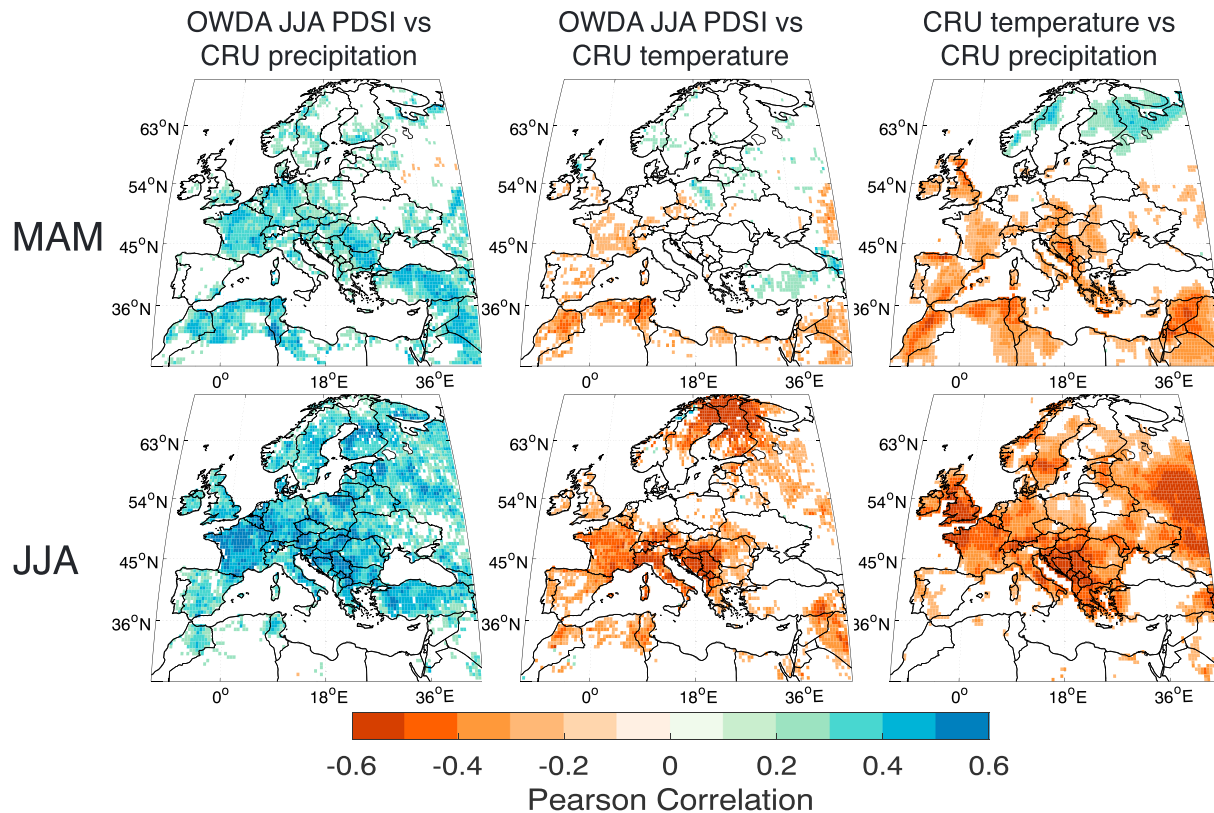
Figure 1. Pearson correlation between (left column) JJA OWDA PDSI and CRU precipitation, (middle column) JJA OWDA PDSI and CRU temperature, and (right column) CRU precipitation and CRU temperature between 1901 and 1978. Only correlations significant at $p < 0.05$ (two-sided Student's t test) shown. (top row) March–May (MAM) and (bottom row) June–August (JJA).

15 year delayed posteruption anomalies with respect to pre-eruption climatology, defined as the mean state over the 5 year period preceding the eruption. The short reference period minimizes the effect of mean background low-frequency climate variability. Since it is likely that some of the "key years" in Table S1 correspond to the same event (e.g., 1168–1169, 1229–1230, 1257–1258, 1344–1345, 1458–1459, 1600–1601, 1694–1695, and 1815–1816), only key years separated by more than 5 years were included in each draw.

We determine the statistical significance of the PDSI, precipitation, and temperature response using SEA by bootstrapped resampling [*Haurwitz and Brier*, 1981]. This is done by comparing the posteruption response to the likelihood of random occurrence, by generating ($n_3 = 10000$) sequences of ($n_2 = 10$) "pseudo key year" samples treated in the same fashion as the actual volcanic key years, including checking that key years chosen in sequences are separated by more than 5 years. We consider epochal anomalies to be significant if the "actual response" either falls below the 5th percentile or is greater than the 95th percentile (i.e., one-sided epochal anomaly at $p < 0.05$).

To evaluate whether volcanically forced hydroclimate observed in the SEA analysis could be modulated though teleconnection patterns (e.g., NAO, EAP, SNAO, and EAWR), we calculate spatial field correlations between these teleconnection patterns and both CRU instrumental precipitation and OWDA PDSI. All temporal correlations are calculated on linearly detrended data and significance is calculated after adjusting the sample size for temporal first-order autocorrelation [*Bretherton et al.*, 1999].

Based on the results of these preliminary analyses (not shown), we present the spatial field correlation between mean April through July (AMJJ) EAP and MSLP over Europe between 1950 and 2012. We then compute the pattern correlation between the SEA response to volcanic forcing and PDSI anomalies forced by the EAP. We adjust the sample size ($n = 5414$ grid cells) used to estimate significance using a 5×5 Gaussian
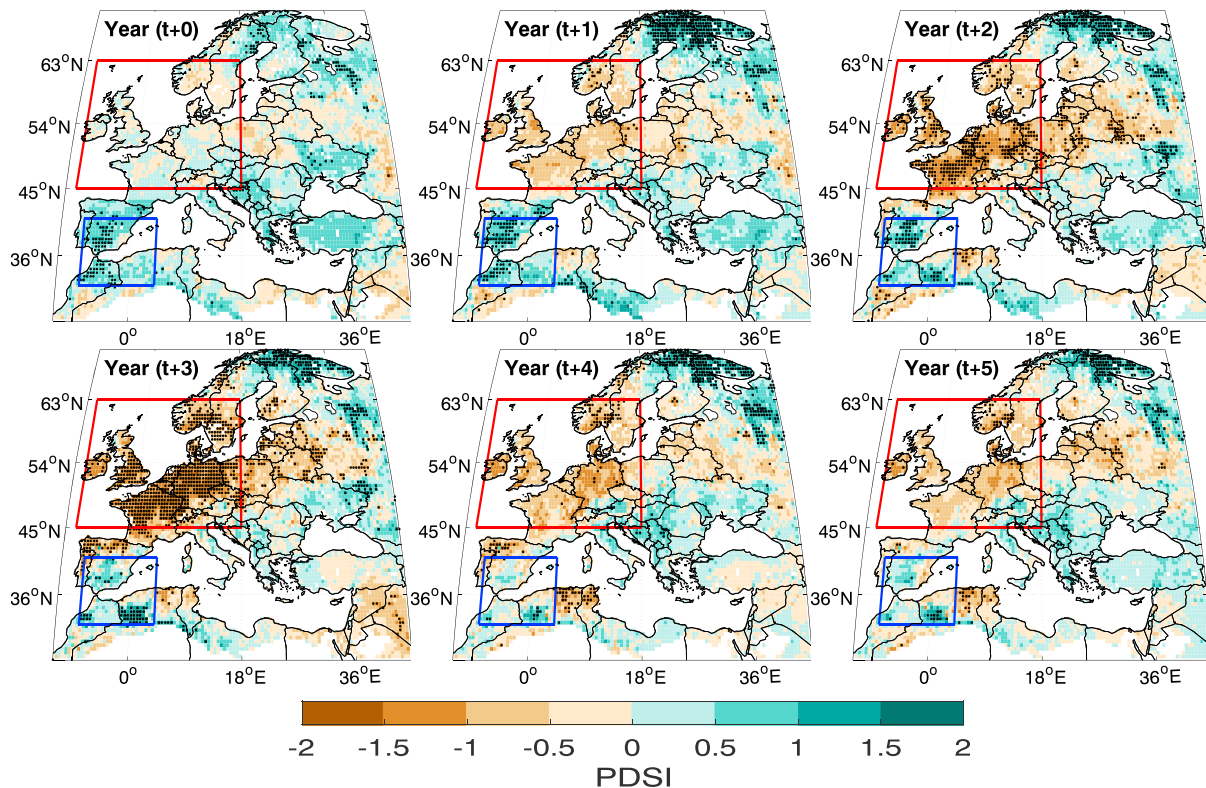
Figure 2. Superposed epoch analysis (SEA) showing OWDA JJA PDSI response to volcanic forcing for years $t + 0$ through $t + 5$ between 1100 and 2012 C.E. Response is the median value for each grid cell. Stipples indicate statistically significant ($p < 0.05$, one-tailed) epochal anomalies.

kernel weighting matrix ($\sigma = 1$) to account for spatial autocorrelation in the PDSI and precipitation fields [*Cliff and Ord*, 1981]. Finally, we develop an estimate of EAP variability for the period 1766–1949, prior to the availability of the reanalysis data, using rotated principal components analysis [*Barnston and Livezey*, 1987] on a reconstruction of 500 hPa geopotential heights (GPH) developed by *Casty et al.* [2007] (see Text S1 for details) [*Raible et al.*, 2014]. We use this estimated EAP series to examine the posteruptive EAP response following the large nineteenth century volcanic eruptions.

3. Results

Over the 1901–1978 period, JJA PDSI correlates significantly ($p < 0.05$, two-sided Student's t test) with both concurrent and antecedent precipitation and temperature (Figures 1 and S1). Precipitation is positively and significantly correlated with JJA PDSI in all seasons over much of the domain, with JJA precipitation showing the strongest signal. Correlations over the Mediterranean are most significant during spring (March through May—MAM), the main season of moisture supply relevant to tree growth in this region (Figure S2). Over the Mediterranean, this relationship is leveraged primarily by May precipitation, while over northwestern Europe the JJA signal is predominantly a reflection of June and July precipitation (not shown). Temperature is negatively correlated with PDSI, especially during JJA (Figure 1, middle column), reflecting either the direct impact of temperature on PDSI (i.e., higher temperatures translate to increased evapotranspiration and lower soil moisture) or the strong inverse correlation during JJA between temperature and precipitation (or soil moisture) over much of the region (Figures 1 (right column) and S1 (right column)) [*Casty et al.*, 2007; *Fischer et al.*, 2007a; *Seneviratne et al.*, 2006].

In the immediate years following an eruption, the median bootstrap hydroclimate response in the OWDA is widespread and significant ($p < 0.05$, one-tailed epochal anomaly) (Figure 2). In the western Mediterranean, pluvial anomalies peak during the event year (year $t + 0$) and 1 year after (year $t + 1$) but persist up to 3 years posteruption (year $t + 3$) (Figure 3a). Conversely, a large and somewhat delayed drying signal emerges over northwestern Europe and the British Isles, peaking 2 to 3 years posteruption (years $t + 2$ and $t + 3$) (Figure 3b).
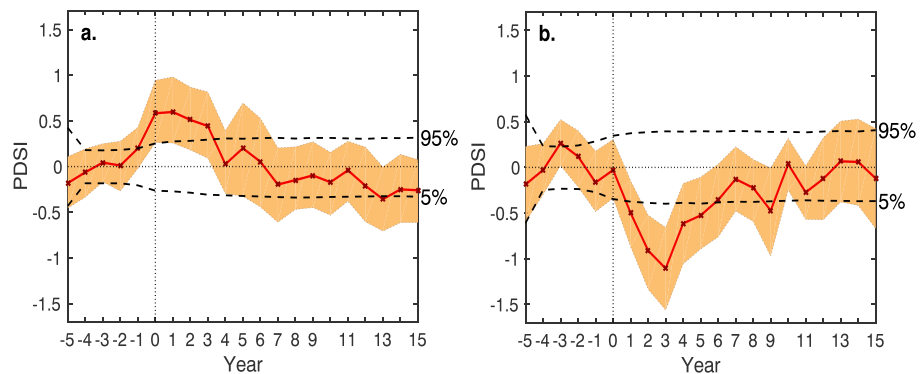
Figure 3. SEA showing area-weighted mean PDSI response over (a) western Mediterranean (blue box—Figure 2) and (b) northwestern Europe (red box—Figure 2). Uncertainty intervals are 10th and 90th percentiles of the response. Dashed horizontal line indicates threshold required for statistically significant ($p < 0.05$, one-tailed) epochal anomalies.

These results are further supported by analysis of the 10th percentile response over the western Mediterranean and the 90th percentile response over northwestern Europe (Figures 3 and S3). Thus, even the driest years posteruption over the western Mediterranean are relatively wet, and the wettest years posteruption over northwestern Europe are relatively dry, compared to pre-eruption values. While persistent positive PDSI anomalies are observed over northern Fennoscandia in years $t + 1$ through $t + 3$ (Figure 2), this response may be a combination of wetting and posteruption cooling, as the OWDA also shows strong summer temperature sensitivity over Fennoscandia (Figure 1).

The median response to volcanic forcing in MAM precipitation [*Pauling et al.*, 2006] shows significant wetting ($p < 0.05$, one-tailed epochal anomaly) over the western Mediterranean 2 years (year $t + 2$) following an eruption (Figure S4). Over northwestern Europe and the British Isles a significant ($p < 0.05$, one-tailed epochal anomaly) reduction in summer JJA precipitation is observed 3 and 4 years (years $t + 3$ and $t + 4$) after an eruption (Figure S5) [*Fischer et al.*, 2007b]. Following an eruption, summer JJA temperatures show significant cooling across the entire region, as documented previously (Figure S6) [*Luterbacher et al.*, 2016].

The EAP is a prominent mode of climate variability over the North Atlantic after the NAO. It appears as a leading mode through the year and is characterized by a northwest-southeast dipole of pressure centers [*Barnston and Livezey*, 1987; *Schrier et al.*, 2006]. It is positively correlated with precipitation over northwestern Europe, the British Isles, and southern Fennoscandia in MAM and JJA and inversely correlated with MAM precipitation in the western Mediterranean and JJA precipitation over southern Iberia (Figure 4, left column). In MAM, a positive EAP is linked to lower than normal MSLP along the European Atlantic sector and anomalously high MSLP around the Mediterranean basin that suppresses precipitation in the region (Figure 4, right column). During a positive EAP the low pressure centered near Scotland intensifies during JJA.

The spatial correlation between the mean AMJJ EAP index and JJA OWDA PDSI between 1950 and 1978 is shown in Figure 5a. A positive phase of the EAP corresponds to wet conditions over northwestern Europe and the British Isles and dry conditions over the western Mediterranean basin. Drying is strongest over southern Iberia, northern Morocco, and northern Algeria. The spatial pattern of PDSI conditions following volcanic eruptions (Figure 2) strongly resembles a negative phase of the EAP, especially in posteruption years $t + 1$, 2, and 3, suggesting that volcanic forcing may modulate spring and summer climate over Europe by stimulating a negative EAP-like atmospheric response. The Pearson correlations between the years $t + 1$, 2, and 3 response (Figure 2) with the EAP-OWDA pattern are $r = -0.47$, -0.44, and -0.52, respectively ($p = 0$, $N' = 686$; $p = 0$, $N' = 589$; and $p = 0$, $N' = 581$, respectively, two-sided Student's t test, N'-sample size adjusted for spatial autocorrelation). Other teleconnection patterns such as the NAO, SNAO, and the EAWR were tested for their influence on hydroclimate over Europe and were not found to force hydroclimate responses spatially similar to that observed following volcanic eruptions.

The NOAA-CPC AMJJ EAP time series between 1950 and 2016 (in red) and the estimated AMJJ EAP between 1800 and 2002 using the *Casty et al.* [2007] 500 hPa GPH reconstruction (in black) are shown in Figure 5b. The two series are significantly correlated during the period of overlap between 1950 and 2002 ($r = 0.71$, $p = 0.0001$, $N = 53$, $N' = 50$ (for temporal autocorrelation), two-sided Student's t test). The inset shows the
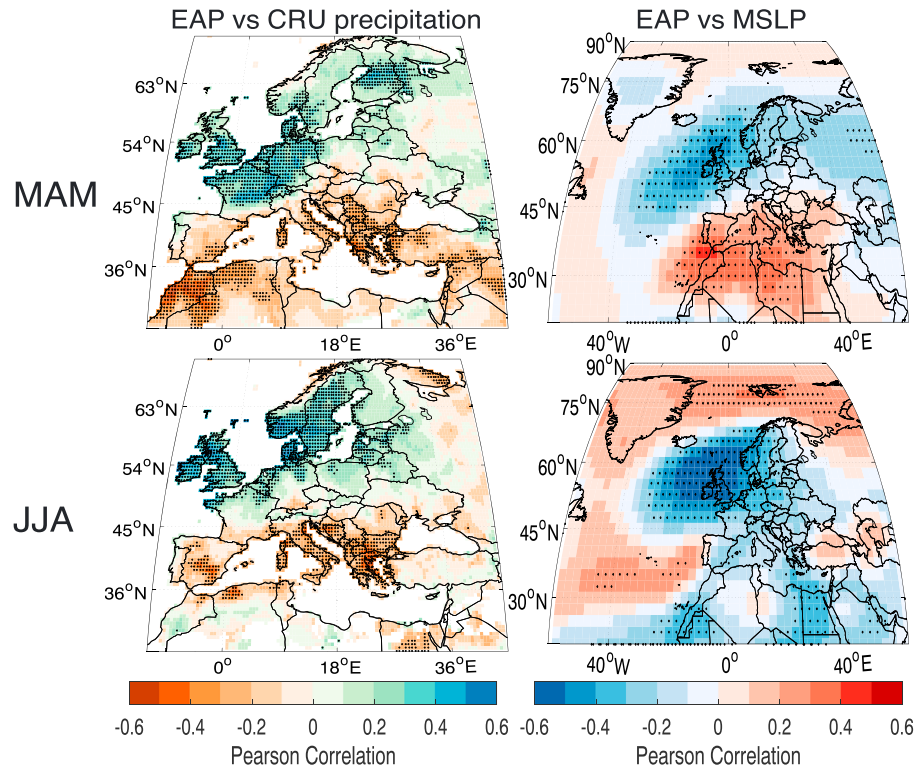
Figure 4. Correlation between East Atlantic Pattern (left column) (EAP) and (right column) CRU precipitation NCAR-NCEP mean sea level pressure (MSLP) for (top row) MAM and (bottom row) JJA between 1950 and 2012. Stippling indicates significant correlation ($p < 0.05$, two-sided, Student's t test). Note different color bars.

posteruption AMJJ EAP response after El Chichón in 1982 (blue line) and Mount Pinatubo in 1991 (green line) after subtracting the 5 year pre-event NOAA-CPC mean EAP index and estimated EAP response following the unknown event in 1809 (grey line), Tambora in 1815 (yellow line), Babuyan in 1831 (pink), Cosiguina in 1835 (olive), and Krakatau in 1884 (based on radiative forcing—black line) after subtracting the 5 year pre-event estimated EAP index. While variability in posteruption EAP and estimated EAP response is high, there is a clustering of negative values at year $t + 0$ and in four out of five cases in year $t + 1$ and $t + 2$. It should be noted, however, that the response after El Chichón is mostly positive.
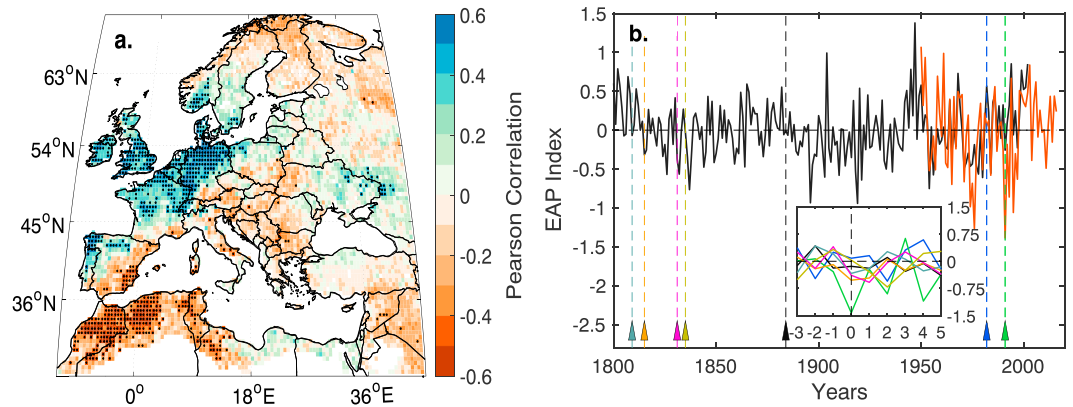
Figure 5. EAP and European hydroclimate. (a) Correlation between April and July (AMJJ) NOAA-CPC EAP index and OWDA JJA PDSI between 1950 and 1978. Stippled blue (red) shading indicates significant positive (negative) correlation ($p < 0.05$, two-sided Student's t test). (b) AMJJ NOAA-CPC EAP index between 1950 and 2016 (red) and estimated from *Casty et al.* [2007] 500 hPa reconstruction (black—see Text S2). Inset shows 5 year posteruptive AMJJ EAP response after 1809 (grey), 1815 (yellow), 1831 (pink), 1835 (olive), 1884 (black), 1982 (blue), and 1991 (green) after subtracting 5 year pre-event mean.

4. Discussion

While postvolcanic spring and summer cooling is a consistent response both regionally (Figure S5) [*Esper et al.*, 2013; *Luterbacher et al.*, 2016] and globally [*D'Arrigo et al.*, 2009; *Stoffel et al.*, 2015], here we show that the hydroclimate response to volcanic forcing is much more spatially heterogeneous [e.g., *Anchukaitis et al.*, 2010]. Posteruption hydroclimate anomalies (Figure 2) over Europe and the Mediterranean resemble those caused by a negative phase of the EAP (Figures 4 and 5a), with pluvial conditions over the western Mediterranean and drought conditions over northwestern Europe and the British Isles (Figures 2 and 3) [also see *Büntgen et al.*, 2017; *Gao and Gao*, 2017]. A similar response is observed in a largely independent seasonal precipitation reconstruction (Figures S4 and S5) [*Fischer et al.*, 2007b] and also simulated, albeit with slightly northward displaced anomalies, in volcanically forced mean May through September precipitation by the Community Earth System Model [*Colose et al.*, 2016, Figure 4].

The hydroclimate system has a high degree of internal spatiotemporal variability. At the same time, there are also uncertainties in the volcanic eruption years themselves [*Baillie*, 2008; *Plummer et al.*, 2012; *Sigl et al.*, 2015]. To account for this uncertainty, we use a novel form of the SEA with nonrepeating subsets of eruption years from a larger key year list (Table S1). Thus, we are able to examine the degree of variability in the hydroclimate system based on different choices of key event years (Figures 3 and S3) and incorporate this uncertainty into our results.

Our analyses suggest that volcanic impacts on spring-summer European hydroclimate are likely modulated by predisposing the EAP toward its negative phase [*Zanchettin et al.*, 2012]. While the mechanisms for this are still uncertain, one possibility examined in model simulations suggests that its causes may originate in the tropics. Following an eruption, a reduction in shortwave radiation at the surface causes faster cooling over land compared to oceans due to the former's lower heat capacity. This reduces the land-sea thermal contrast, weakening monsoon circulations including the West African monsoon [*Joseph and Zeng*, 2011]. In turn, the weakened monsoonal precipitation and equatorial convergence reduces latent heat fluxes in the free troposphere and weakens the Hadley and Ferrel cell circulations [*Rind et al.*, 1992]. Using the European Centre/Hamburg 5.4 model *Wegmann et al.* [2014] found that weakening these circulations weakens the meridional pressure gradient in the North Atlantic, causing southward shifted storm tracks and anomalous uplift over the Mediterranean that increased convection and precipitation over the Mediterranean. Our findings (Figures 2–5) suggest that the hydroclimate response to volcanic forcing is consistent with this hypothesized weakening of the descending branch of the Hadley circulation and southward shift of storm tracks, causing springtime wetting over the western Mediterranean and spring and summer drying over northwestern Europe. Although this mechanism is largely consistent with that proposed by *Gao and Gao* [2017], we show that the OWDA primarily reflects spring through summer soil moisture (Figures 1 and S1). Thus, it is unlikely that volcanically induced wintertime teleconnection anomalies, such as a positive winter NAO, play a dominant role in influencing the observed response. Based on these dynamics and the resemblance between hydroclimate anomalies induced by volcanic eruptions (Figure 2) and those triggered by the EAP (Figures 4 and 5), this theory offers at least a plausible physical mechanism for volcanic forcing of spring-summer hydroclimate over Europe and the Mediterranean by inducing a negative phase of the EAP.

5. Conclusions

We used a new millennium-length tree ring-based hydroclimate reconstruction with an expanded event year list and a novel modification to SEA, to demonstrate a robust but spatially complex response of European and Mediterranean hydroclimate to volcanic eruptions. The forced hydroclimate response appears to be triggered by a negative phase of the EAP which causes anomalous spring uplift over the western Mediterranean, southward shifted storm tracks, and a weakened spring-summer meridional pressure gradient over the North Atlantic. Consequently, we observe wetting over the western Mediterranean and drying over northwestern Europe following volcanic eruptions. However, the exact dynamical mechanisms by which volcanic eruptions trigger this response (e.g., possibly by weakening equatorial convergence and the West African monsoon) still need to be better understood. These results highlight the complexity of hydroclimate response to eruptions and suggest the need to consider carefully how aerosol forcing (e.g., from volcanoes, pollution, or geoengineering) may modulate hydroclimate in the future.

References

Adams, J. B., M. E. Mann, and C. M. Ammann (2003), Proxy evidence for an El Niño-like response to volcanic forcing, *Nature*, 426(6964), 274–278.

Anchukaitis, K. J., B. Buckley, E. Cook, B. Cook, R. D'Arrigo, and C. Ammann (2010), Influence of volcanic eruptions on the climate of the Asian monsoon region, *Geophys. Res. Lett.*, 37, L22703, doi:10.1029/2010GL044843.

Anchukaitis, K. J., et al. (2012), Tree rings and volcanic cooling, *Nat. Geosci.*, 5(12), 836–837.

Anchukaitis, K. J., et al. (2017), Last millennium Northern Hemisphere summer temperatures from tree rings: Part II, spatially resolved reconstructions, *Quat. Sci. Rev.*, 163, 1–22.

Baillie, M. G. (2008), Proposed re-dating of the European ice core chronology by seven years prior to the 7th century AD, *Geophys. Res. Lett.*, 35, L15813, doi:10.1029/2008GL034755.

Barnston, A. G., and R. E. Livezey (1987), Classification, seasonality and persistence of low-frequency atmospheric circulation patterns, *Mon. Weather Rev.*, 115(6), 1083–1126.

Bretherton, C. S., M. Widmann, V. P. Dymnikov, J. M. Wallace, and I. Bladé (1999), The effective number of spatial degrees of freedom of a time-varying field, *J. Clim.*, 12(7), 1990–2009.

Broccoli, A. J., K. W. Dixon, T. L. Delworth, T. R. Knutson, R. J. Stouffer, and F. Zeng (2003), Twentieth-century temperature and precipitation trends in ensemble climate simulations including natural and anthropogenic forcing, *J. Geophys. Res.*, 108(D24), 4798, doi:10.1029/2003JD003812.

Büntgen, U., et al. (2017), New tree-ring evidence from the Pyrenees reveals western Mediterranean climate variability since medieval times, *J. Clim.*, doi:10.1175/JCLI-D-16-0526.1.

Casty, C., C. C. Raible, T. F. Stocker, H. Wanner, and J. Luterbacher (2007), A European pattern climatology 1766–2000, *Clim. Dyn.*, 29(7–8), 791–805.

Cliff, A. D., and J. K. Ord (1981), Spatial and temporal analysis: Autocorrelation in space and time, in *Quantitative Geography: A British View*, pp. 104–110, Routledge, London.

Colose, C. M., A. N. LeGrande, and M. Vuille (2016), Hemispherically asymmetric volcanic forcing of tropical hydroclimate during the last millennium, *Earth Syst. Dyn.*, 7(3), 681–696.

Cook, E. R., D. M. Meko, D. W. Stahle, and M. K. Cleaveland (1999), Drought reconstructions for the continental United States*, *J. Clim.*, 12(4), 1145–1162.

Cook, E. R., et al. (2015), Old world megadroughts and pluvials during the Common Era, *Sci. Adv.*, 1(10) e1500561.

Crowley, T., and M. Unterman (2013), Technical details concerning development of a 1200 yr proxy index for global volcanism, *Earth Syst. Sci. Data*, 5(1), 187–197.

D'Arrigo, R., R. Wilson, and A. Tudhope (2009), The impact of volcanic forcing on tropical temperatures during the past four centuries, *Nat. Geosci.*, 2(1), 51–56.

Dai, A. (2011), Characteristics and trends in various forms of the Palmer Drought Severity Index during 1900–2008, *J. Geophys. Res.*, 116, D12115, doi:10.1029/2010JD015541.

Driscoll, S., A. Bozzo, L. J. Gray, A. Robock, and G. Stenchikov (2012), Coupled Model Intercomparison Project 5 (CMIP5) simulations of climate following volcanic eruptions, *J. Geophys. Res.*, 117, D17105, doi:10.1029/2012JD017607.

Esper, J., L. Schneider, P. J. Krusic, J. Luterbacher, U. Büntgen, M. Timonen, F. Sirocko, and E. Zorita (2013), European summer temperature response to annually dated volcanic eruptions over the past nine centuries, *Bull. Volcanol.*, 75(7), 1–14.

Fischer, E., S. Seneviratne, P. Vidale, D. Lüthi, and C. Schär (2007a), Soil moisture-atmosphere interactions during the 2003 European summer heat wave, *J. Clim.*, 20(20), 5081–5099.

Fischer, E., J. Luterbacher, E. Zorita, S. Tett, C. Casty, and H. Wanner (2007b), European climate response to tropical volcanic eruptions over the last half millennium, *Geophys. Res. Lett.*, 34, L05707, doi:10.1029/2006GL027992.

Folland, C. K., J. Knight, H. W. Linderholm, D. Fereday, S. Ineson, and J. W. Hurrell (2009), The summer North Atlantic Oscillation: Past, present, and future, *J. Clim.*, 22(5), 1082–1103.

Fritts, H. (1976), *Tree Rings and Climate*, chap. 1, 26 pp., Academic Press, San Diego, Calif.

Gao, C., A. Robock, and C. Ammann (2008), Volcanic forcing of climate over the past 1500 years: An improved ice core-based index for climate models, *J. Geophys. Res.*, 113, D23111, doi:10.1029/2008JD010239.

Gao, Y., and C. Gao (2017), European hydroclimate response to volcanic eruptions over the past nine centuries, *Int. J. Climatol.*, doi:10.1002/joc.5054.

George, S. S., D. M. Meko, and E. R. Cook (2010), The seasonality of precipitation signals embedded within the North American drought Atlas, *The Holocene*, 20(6), 983–988.

Harris, I., P. Jones, T. Osborn, and D. Lister (2014), Updated high-resolution grids of monthly climatic observations—The CRU TS3. 10 dataset, *Int. J. Climatol.*, 34(3), 623–642.

Haurwitz, M. W., and G. W. Brier (1981), A critique of the superposed epoch analysis method: Its application to solar-weather relations, *Mon. Weather Rev.*, 109(10), 2074–2079.

Iles, C. E., and G. C. Hegerl (2014), The global precipitation response to volcanic eruptions in the CMIP5 models, *Environ. Res. Lett.*, 9(10), 104012.

Iles, C. E., G. C. Hegerl, A. P. Schurer, and X. Zhang (2013), The effect of volcanic eruptions on global precipitation, *J. Geophys. Res. Atmos.*, 118, 8770–8786, doi:10.1002/jgrd.50678.

Joseph, R., and N. Zeng (2011), Seasonally modulated tropical drought induced by volcanic aerosol, *J. Clim.*, 24(8), 2045–2060.

Kalnay, E., M. Kanamitsu, R. Kistler, W. Collins, D. Deaven, L. Gandin, M. Iredell, S. Saha, G. White, and J. Woollen (1996), The NCEP/NCAR 40-year reanalysis project, *Bull. Am. Meteorol. Soc.*, 77(3), 437–471.

Luterbacher, J., and C. Pfister (2015), The year without a summer, *Nat. Geosci.*, 8, 246–248.

Luterbacher, J., et al. (2016), European summer temperatures since Roman times, *Environ. Res. Lett.*, 11(2), 024001.

Meehl, G. A., W. M. Washington, C. M. Ammann, J. M. Arblaster, T. Wigley, and C. Tebaldi (2004), Combinations of natural and anthropogenic forcings in twentieth-century climate, *J. Clim.*, 17(19), 3721–3727.

Palmer, W. C. (1965), *Meteorological Drought*, pp. 6–27, US Department of Commerce, Weather Bureau, Washington, D. C.

Pauling, A., J. Luterbacher, C. Casty, and H. Wanner (2006), Five hundred years of gridded high-resolution precipitation reconstructions over Europe and the connection to large-scale circulation, *Clim. Dyn.*, 26(4), 387–405.

Plummer, C., M. Curran, T. D. V. Ommen, S. O. Rasmussen, A. Moy, T. Vance, H. B. Clausen, B. M. Vinther, and P. Mayewski (2012), An independently dated 2000-yr volcanic record from law dome, East Antarctica, including a new perspective on the dating of the 1450s CE eruption of Kuwae, Vanuatu, *Clim. Past*, 8(6), 1929–1940.

Raible, C., F. Lehner, J. F. González Rouco, and L. Fernández Donado (2014), Changing correlation structures of the Northern Hemisphere atmospheric circulation from 1000 to 2100 AD, *Clim. Past*, *10*(2), 537–550.

Rind, D., N. Balachandran, and R. Suozzo (1992), Climate change and the middle atmosphere. Part II: The impact of volcanic aerosols, *J. Clim.*, *5*(3), 189–208.

Robock, A. (2000), Volcanic eruptions and climate, *Rev. Geophys.*, *38*(2), 191–219, doi:10.1029/1998RG000054.

Schrier, G., K. Briffa, P. Jones, and T. Osborn (2006), Summer moisture variability across Europe, *J. Clim.*, *19*(12), 2818–2834.

Schrier, G., J. Barichivich, K. Briffa, and P. Jones (2013), A scPDSI-based global data set of dry and wet spells for 1901–2009, *J. Geophys. Res. Atmos.*, *118*, 4025–4048, doi:10.1002/jgrd.50355.

Seneviratne, S. I., D. Lüthi, M. Litschi, and C. Schär (2006), Land–atmosphere coupling and climate change in Europe, *Nature*, *443*(7108), 205–209.

Shindell, D. T., G. A. Schmidt, M. E. Mann, and G. Faluvegi (2004), Dynamic winter climate response to large tropical volcanic eruptions since 1600, *J. Geophys. Res.*, *109*, D05104, doi:10.1029/2003JD004151.

Sigl, M., et al. (2013), A new bipolar ice core record of volcanism from WAIS divide and NEEM and implications for climate forcing of the last 2000 years, *J. Geophys. Res. Atmos.*, *118*, 1151–1169, doi:10.1029/2012JD018603.

Sigl, M., et al. (2015), Timing and climate forcing of volcanic eruptions for the past 2,500 years, *Nature*, *523*(7562), 543–549.

Stoffel, M., et al. (2015), Estimates of volcanic-induced cooling in the Northern Hemisphere over the past 1,500 years, *Nat. Geosci.*, *8*(10), 784–788.

Wegmann, M., S. Brönnimann, J. Bhend, J. Franke, D. Folini, M. Wild, and J. Luterbacher (2014), Volcanic influence on European summer precipitation through monsoons: Possible cause for "years without summer"*, *J. Clim.*, *27*(10), 3683–3691.

Zanchettin, D., C. Timmreck, H.-F. Graf, A. Rubino, S. Lorenz, K. Lohmann, K. Krüger, and J. Jungclaus (2012), Bi-decadal variability excited in the coupled ocean–atmosphere system by strong tropical volcanic eruptions, *Clim. Dyn.*, *39*(1–2), 419–444.

Zanchettin, D., C. Timmreck, O. Bothe, S. J. Lorenz, G. Hegerl, H. F. Graf, J. Luterbacher, and J. H. Jungclaus (2013), Delayed winter warming: A robust decadal response to strong tropical volcanic eruptions?, *Geophys. Res. Lett.*, *40*, 204–209, doi:10.1029/2012GL054403.